biomedicines

MDPI

Article

Multimodal Quantitative Imaging of the Microvascular Component in Cellulite: Candidate Imaging Biomarkers of Treatment Response

Anna Deda [1,*], Marta Gędoś [2], Martyna Wojciechowska [2], Paula Babczyńska [3], Agata Lebiedowska [3,*], Wiktoria Odrzywołek [3], Magdalena Hartman-Petrycka [3], Aleksandra Lipka-Trawińska [4], Klaudia Mazurek [1], Dominika Wcisło-Dziadecka [1] and Sławomir Wilczyński [3]

[1] Department of Practical Cosmetology and Skin Diagnostics, Faculty of Pharmaceutical Sciences in Sosnowiec, Medical University of Silesia in Katowice, ul. Jedności 8b, 41-200 Sosnowiec, Poland
[2] Student Scientific Society, Department of Practical Cosmetology and Skin Diagnostics, Faculty of Pharmaceutical Sciences in Sosnowiec, Medical University of Silesia in Katowice, 8b Jedności Street, 41-200 Sosnowiec, Poland
[3] Department of Basic Biomedical Sciences, Faculty of Pharmaceutical Sciences in Sosnowiec, Medical University of Silesia in Katowice, ul. Jedności 8b, 41-200 Sosnowiec, Poland; swilczynski@sum.edu.pl (S.W.)
[4] Clinical Department of Dermatology, Department of Internal Medicine, Dermatology and Allergology, Faculty of Medical Sciences in Zabrze, Medical University of Silesia in Katowice, 41-800 Zabrze, Poland
* Correspondence: adeda@sum.edu.pl (A.D.); alebiedowska@sum.edu.pl (A.L.)

Abstract

Background/Objectives: Cellulite is a complex alteration of the dermal–subcutaneous interface involving structural and microvascular components. This study evaluated changes in quantitative imaging parameters following ALIDYA mesotherapy using a multimodal protocol and explored candidate imaging biomarkers potentially reflecting the microvascular component of cellulite. **Methods:** In this prospective, single-arm, exploratory before–after study, thirty women aged 20–45 years with Nürnberger–Müller grade I–IV cellulite of the posterior thighs underwent six weekly ALIDYA mesotherapy sessions. Assessments were performed at baseline (T1), at an intermediate assessment after the third treatment (T2), and at final follow-up (T3). Cross-polarized photography with Gray-Level Co-occurrence Matrix (GLCM) analysis, infrared thermography with GLCM analysis, hyperspectral imaging, and Antera 3D erythema assessment were performed. Longitudinal changes were analyzed using non-parametric methods. **Results:** Photographic GLCM Contrast decreased and Homogeneity increased significantly over time ($p \leq 0.002$). Thermographic Contrast decreased ($p \leq 0.003$), while thermographic Homogeneity increased ($p \leq 0.012$). Hyperspectral HbDepth560 decreased ($p = 0.002$), whereas R560/R650 and R577/R650 increased (both $p < 0.001$). VIS slope increased ($p = 0.016$), while Water970_800 ($p = 0.967$) and NIR slope ($p = 0.792$) remained unchanged. Antera 3D Redness Score and its minimum and maximum values decreased significantly (all $p < 0.001$), whereas Uniformity remained unchanged. Effect sizes (Kendall's W) were largest for the Antera 3D erythema parameters (0.32–0.55) and the hemoglobin-related hyperspectral indices (0.20–0.31) and smallest for the VIS slope (0.14). Treatment was well tolerated; transient bruising with local tenderness at the injection sites was the only adverse event, and no participant discontinued treatment. **Conclusions:** Several optical, thermal and multispectral imaging parameters changed concordantly during the ALIDYA treatment period. These parameters can be regarded as candidate imaging biomarkers of the microvascular component of cellulite that require further validation; without a control group, reproducibility data or direct perfusion measurements, the changes cannot be attributed to a specific mechanism

Academic Editor: Hua Su

Received: 6 October 2026
Revised: 19 October 2026
Accepted: 20 October 2026
Published: 23 October 2026

Copyright: © 2026 by the authors. Licensee MDPI, Basel, Switzerland. This article is an open access article distributed under the terms and conditions of the Creative Commons Attribution (CC BY) license.

of the product or interpreted as evidence of improved microcirculation. The main contribution of the study is methodological: it shows that complementary quantitative imaging techniques can be combined in a single protocol to monitor cellulite-associated tissue changes.

Keywords: cellulite; gynoid lipodystrophy; microcirculation; quantitative imaging; GLCM texture analysis; thermography; hyperspectral imaging; Antera 3D; candidate imaging biomarkers; ALIDYA

1. Introduction

Cellulite (gynoid lipodystrophy, edematous-fibrosclerotic panniculopathy) is one of the most common aesthetic concerns in post-pubertal women, affecting approximately 80–90% of the female population regardless of body mass. Lesions localize mainly to the thighs, buttocks and hips. Unlike obesity, cellulite is a complex process involving the dermis, the dermal–subcutaneous interface and superficial adipose tissue [1,2]. It is now regarded as a multifactorial tissue-remodeling process encompassing microcirculatory impairment, interstitial fluid retention, extracellular matrix (ECM) remodeling, fibrosis of connective tissue septa and adipocyte dysfunction, which together produce the characteristic surface irregularities known as "orange-peel" skin [3].

Remodeling of the ECM and microcirculatory dysfunction reinforce one another rather than occurring independently. Increased glycosaminoglycan and proteoglycan content promotes interstitial water retention, which raises tissue tension, impairs metabolic exchange and, over time, drives fibroblast activation and fibrosis of the connective tissue septa [3–5]. Increased capillary permeability, venous and lymphatic stasis and heterogeneous perfusion in turn cause local hypoxia and alter the thermal and optical properties of the skin [3,6]. Oxidative stress and adipocyte dysfunction add a local metabolic-inflammatory component to this process [3,5]. This complexity is one of the reasons why objective, quantitative methods are needed to monitor the response to therapy.

Cellulite severity is most often graded with visual and palpation scales such as the Nürnberger–Müller classification and the Cellulite Severity Scale. These scales are subjective and depend on examiner experience as well as on lighting, body position and muscle tension. They also have limited sensitivity to the small changes that occur during treatment, particularly early on, when any improvement may concern mainly the microcirculation and tissue remodeling rather than the visible relief of the skin [1,7]. Objective imaging methods are therefore increasingly important for reliable monitoring of anti-cellulite therapy [3].

Several imaging techniques provide quantitative, operator-independent information on the skin changes associated with cellulite. Texture analysis of digital photographs with the Gray-Level Co-occurrence Matrix (GLCM) proposed by Haralick et al. describes the spatial relationships between neighboring pixels; in cellulite, high Contrast reflects marked surface heterogeneity, whereas increasing Homogeneity indicates smoothing of the skin surface [6,8]. Infrared thermography records the distribution of skin surface temperature, which depends on cutaneous blood flow and tissue metabolism; in cellulite, venous and lymphatic stasis produce a mosaic "leopard-skin" thermal pattern, and GLCM analysis of thermograms is more informative than mean temperature alone [3,6]. Hyperspectral imaging (HSI) records a full reflectance spectrum for every pixel [9]. The main skin chromophores are hemoglobin, melanin and water [10]: the 500–600 nm range corresponds to the absorption bands of hemoglobin, 700–900 nm carries information from deeper layers and the region around 970 nm is associated with water absorption [11,12].

Indices derived from these spectral regions therefore reflect the hemoglobin and water content and the scattering properties of the tissue [10,13,14]. Finally, the Antera 3D system uses multispectral illumination and three-dimensional reconstruction to separate the optical contributions of hemoglobin and melanin, enabling reproducible quantification of erythema [15].

Each of these modalities provides complementary information. It should be emphasized, however, that none of them measures blood flow directly. Texture, thermal and spectral parameters are indirect surrogate measures that reflect the optical and thermal consequences of altered superficial perfusion, interstitial edema and tissue remodeling. Their combination may nevertheless characterize the microvascular component of cellulite more comprehensively than any single technique and may help to identify candidate quantitative biomarkers of treatment response [3,6].

ALIDYA is an injectable medical device marketed for the treatment of cellulite. Its formulation contains ethylenediaminetetraacetic acid (EDTA), a chelator of metal ions, together with amino acids, a gelatin hydrolysate and buffering components. The proposed rationale is that chelation of transition-metal ions limits reactions generating reactive oxygen species and thereby reduces local oxidative stress, and that the product supports microcirculation and reduces venous–lymphatic stasis [3–5]. These mechanisms have been inferred mainly from the known properties of EDTA and have not been demonstrated directly in cellulite tissue; they should therefore be regarded as hypotheses rather than established effects. Instrumental methods such as thermography and image texture analysis have previously proved sensitive to treatment-related changes in cellulite [6,16], but objective imaging data on ALIDYA remain scarce, and no study has so far combined thermal, optical and spectral measurements to characterize its effect on the microvascular component.

To our knowledge, no study has integrated GLCM texture analysis of cross-polarized photographs, infrared thermography, hyperspectral imaging and Antera 3D erythema analysis within a single protocol to evaluate the microvascular component of cellulite, and none has done so for ALIDYA. The aim of this prospective, single-arm study was therefore to characterize the changes in quantitative imaging parameters related to the microvascular component of cellulite during and after a series of ALIDYA mesotherapy sessions, and to explore which of these parameters may serve as candidate imaging biomarkers of treatment response. Because the study had no control group and no reference measurement of cutaneous perfusion, it was designed as an exploratory, hypothesis-generating investigation, and the results are interpreted accordingly. Structural and subcutaneous outcomes obtained in the same cohort (three-dimensional morphometry of skin depressions, high-frequency ultrasound of the dermis and clinical grading) will be reported separately; the present analysis complements that report by focusing on the optical and thermal parameters related to the microvascular component.

2. Materials and Methods

2.1. Study Design

This study was designed as a prospective, single-arm, non-randomized before–after study evaluating longitudinal changes in imaging parameters during and after ALIDYA (Marllor Biomedical, Italy) mesotherapy. All participants underwent the same six-session treatment protocol and were assessed at three predefined time points: T1, at baseline before the first treatment; T2, at the intermediate assessment after the third treatment, approximately one month after the first treatment; and T3, at the final follow-up, six weeks after the sixth and final treatment and approximately three months after the first treatment (Figure 1). The study was open-label; because no comparator was available, neither participants nor investigators were blinded to the intervention. All imaging parameters

analyzed in this study are indirect surrogate measures of the microvascular component of cellulite: none of the methods used measures cutaneous blood flow directly, and no reference perfusion technique (laser Doppler flowmetry, laser speckle contrast imaging, color Doppler ultrasonography or capillaroscopy) was applied.

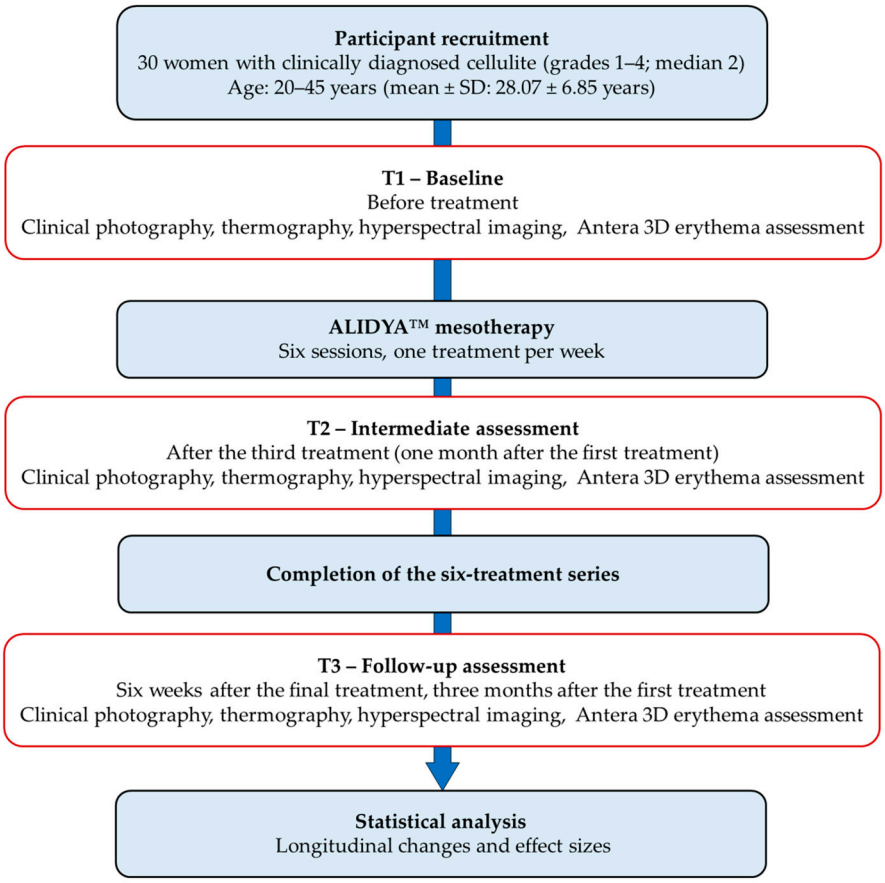


Figure 1. Study design and timeline of ALIDYA mesotherapy and imaging assessments. Data are presented as mean ± standard deviation (SD).

2.2. Study Group

Thirty women aged 20–45 years (mean 28.07 ± 6.85 years) with Nürnberger–Müller grade I-IV cellulite on the posterior thighs were enrolled; lesions were confirmed by clinical examination comprising visual assessment in the standing position and palpation. Inclusion criteria were female sex, age 20–45 years, clinically diagnosed cellulite, stable body weight in the period preceding the study, no contraindications to mesotherapy, and informed consent to participation and to photographic and imaging documentation. Exclusion criteria were pregnancy or breastfeeding, clinically significant systemic disease, coagulation disorders, treatment with immunosuppressants or systemic corticosteroids, a history of thromboembolic disease, clinically significant chronic venous insufficiency, implanted devices in the treatment area, and concurrent invasive or non-invasive anti-cellulite treatment. All participants underwent six ALIDYA mesotherapy sessions at 7-day intervals, as described in Section 2.3. Assessments were performed prospectively at three predefined time points: T1, at baseline before the first ALIDYA treatment; T2, at the intermediate assessment after the third treatment, approximately one month after the first treatment; and T3, at the final follow-up, six weeks after the sixth and final treatment and approximately three months after the first treatment.

No a priori sample-size calculation or power analysis was performed. The sample size was determined by study feasibility, and the analyses were therefore considered exploratory rather than confirmatory.

The study was conducted in accordance with the Declaration of Helsinki and approved by the Ethics Committee of Medical University of Silesia, Katowice (KNW/0022/KB1/27/I/16). The study was registered retrospectively at ClinicalTrials.gov (NCT07675356; first posted 30 June 2026), after recruitment and the intervention had been completed. The registered primary outcome, the change in Nürnberger–Müller grade at three months, together with the structural imaging outcomes, will be reported in a separate publication; the imaging parameters analyzed here were registered as secondary outcomes, and none of them was designated as a primary endpoint. All participants provided written informed consent prior to enrollment.

2.3. Intervention

ALIDYA (Marllor Biomedical, Italy) is supplied as a kit containing one vial of lyophilisate (340 mg) and one vial of 10 mL of solvent. According to the manufacturer, the lyophilisate contains polyamino acids, gelatin hydrolysate, mannitol, calcium ascorbate, amino acids, EDTA, β-cyclodextrin, sodium chloride and sodium bicarbonate. The product was reconstituted immediately before use according to the manufacturer's instructions. All participants received six treatment sessions at 7-day intervals. At each session, after disinfection of the skin, the solution was administered to the posterior surface of both thighs by needle mesotherapy, using point-by-point microinjections into the deep dermis or the upper subcutaneous layer at a depth of approximately 4 mm, with a 30G × 4 mm needle, at intervals of approximately 1.5 cm, delivering 0.05–0.1 mL per injection point. The total volume per session depended on body weight: 10 mL (5 mL per thigh) in participants weighing less than 70 kg and 20 mL (10 mL per thigh) in those weighing 70 kg or more. No topical anesthesia was used, and participants were asked only to avoid sun exposure and intensive physical exercise on the day of treatment. All procedures were performed by the same experienced operator (A.D.) using the same technique at the AJ Med clinic in Mysłowice, Poland, whereas all imaging examinations were performed at the Faculty of Pharmaceutical Sciences in Sosnowiec. Participants were instructed not to use any other anti-cellulite treatment or topical product on the thighs for the duration of the study. Imaging at T2 was performed immediately before the next treatment session, i.e., at least seven days after the preceding injections, to minimize the influence of acute post-injection reactions on the measurements.

2.4. Photography

Photographic documentation was performed with a validated Fotomedicus system (Elfo, Poland) equipped with a high-resolution digital camera and a ring light source with high color rendering (CRI > 90). All images were acquired under standardized conditions with identical patient positioning, constant lens distance and a uniform matte background; a positioning mat ensured reproducible placement, enabling comparison of images obtained at T1, T2 and T3. Participants stood with their feet on fixed markers of the positioning mat, with the arms relaxed and the thigh muscles not tensed; the camera height, the camera-to-subject distance and the framing were fixed by the system, and the camera settings (focal length, aperture, exposure time, ISO and white balance) were kept constant for all acquisitions. All photographs were acquired by the same operator. Cross-polarized light (90°) was obtained using two linear polarizing filters placed on the lens and on the light source, eliminating surface reflections from the stratum corneum and the hydrolipidic film and allowing for more accurate assessment of skin texture. Images were saved in lossless RAW format to preserve full pixel information and imported into

MATLAB R2023b (version 23.2), where topographically identical regions of interest (ROIs) covering the treated area were defined as the basis for quantitative texture analysis.

2.5. GLCM Texture Analysis

Texture analysis was performed in MATLAB using the Gray-Level Co-occurrence Matrix (GLCM) algorithm. For each image, topographically identical ROIs covering the treated area were defined; the ROI coordinates established at T1 were retained and reused for the analyses at T2 and T3 to ensure comparability. A rectangular ROI was placed on the posterior surface of each thigh on the baseline image by a single investigator (S.W.), using the gluteal fold and the popliteal crease as anatomical landmarks; because the images were acquired in the same frame of reference, the saved coordinates could be applied to the T2 and T3 images without modification, and correct placement was verified visually on each follow-up image. Images were converted to 8-bit grayscale, and the GLCM was computed for a pixel distance of 1 and averaged over four directions (0°, 45°, 90° and 135°). Because the texture parameters are computed algorithmically within the predefined ROI, their calculation involves no subjective visual scoring. Two texture parameters were computed: Contrast, describing local variation in image brightness and reflecting surface heterogeneity (higher values indicate more pronounced irregularities), and Homogeneity, describing image uniformity (higher values indicate a smoother surface). Changes in both parameters were used as quantitative descriptors of skin-surface texture.

2.6. Thermography

Thermographic imaging was performed with a FLIR T420sc camera (FLIR Systems, USA) equipped with an uncooled microbolometer focal-plane-array detector recording infrared radiation in the 7.5–13 μm range, with a resolution of 320 × 240 pixels and a thermal sensitivity NETD < 0.045 K. The camera was tripod-mounted with the lens perpendicular to the skin surface at a distance of about 50 cm. Measurements were performed under standardized environmental conditions (22 ± 4 °C, relative humidity 40 ± 15%) after at least 20 min of acclimatization to stabilize skin surface temperature. The camera was factory-calibrated; skin emissivity was set to 0.98, and the ambient temperature and relative humidity were entered into the camera before each session. Participants acclimatized undressed from the waist down in the standing position and were asked to refrain from intensive physical exercise, hot beverages, alcohol and smoking for at least two hours before the measurement. Thermograms were exported as radiometric temperature matrices and processed in MATLAB; the ROIs were defined on the baseline thermogram using the same anatomical landmarks as for photography and transferred to the follow-up thermograms. Thermograms were analyzed within identically defined ROIs using the GLCM algorithm; Contrast (local variation in the temperature distribution) and Homogeneity (thermogram uniformity) were computed as indirect descriptors of the spatial distribution of skin surface temperature, which depends on, but is not a direct measure of, cutaneous blood flow.

2.7. Hyperspectral Imaging

Hyperspectral imaging was performed with a SPECIM IQ camera (Specim, Finland) recording images over the 400–1000 nm wavelength range (204 spectral bands, spectral resolution of about 7 nm, 512 × 512 pixels) under standardized illumination, with a constant camera-to-skin distance and identical positioning across all visits. Before each acquisition the camera was calibrated against the manufacturer's white reference tile placed in the field of view, and the dark current was recorded with the shutter closed; reflectance was calculated for every pixel and wavelength as (raw − dark)/(white − dark). For each measurement an ROI covering the treated area was analyzed at T1, T2 and T3.

Hyperspectral indices were computed for a single ROI per participant averaged over both thighs; consequently, one set of hyperspectral values per participant and time point is reported, without separation into the left and right thigh. Reflectance spectra were averaged within the ROI before the indices were computed. From the reflectance spectra, hemoglobin-related indices were derived: HbDepth560, defined as the depth of the hemoglobin absorption feature at 560 nm relative to a linear baseline fitted between 510 and 610 nm, and the reflectance ratios R560/R650 and R577/R650, which relate the reflectance at the oxyhemoglobin absorption bands to the reflectance at 650 nm, where hemoglobin absorption is low. Water-related absorption was assessed by the Water970_800 index, the ratio of the reflectance at 970 nm to that at 800 nm, and tissue reflectance by the VIS slope and NIR slope, defined as the slopes of linear fits to the reflectance curve in the 500–600 nm and 700–900 nm ranges, respectively. All parameters were computed within the same ROIs to enable quantitative assessment of treatment-related changes in the optical properties of the skin. HbDepth560 and the two reflectance ratios are dominated by hemoglobin absorption in the superficial dermis, but they are also influenced by melanin absorption, by tissue scattering and by the oxygenation state of hemoglobin; they are therefore reported as hemoglobin-related indices and not as measures of hemoglobin concentration (see Section 4). The Water970_800 index is computed in a spectral region where the absorption band of water is weak, where the sensitivity of the camera sensor decreases and where the sampling depth of light reaches several millimeters; its sensitivity to changes in the interstitial fluid content of the dermis is therefore limited.

2.8. Antera 3D Analysis

Skin imaging was performed with the Antera 3D® system (Miravex Ltd., Dublin, Ireland), which uses multispectral illumination and three-dimensional surface reconstruction. Imaging was performed under standardized conditions with identical positioning of the participants and a constant measurement field across all visits, analyzing the same ROIs on the posterior thighs. The device performs an internal calibration before each acquisition; the measurement head (field of view 56 × 56 mm) was placed perpendicularly on the skin, without pressure, at positions marked relative to the gluteal fold and recorded on a body chart to allow for repositioning at the follow-up visits. Parameters were computed with the manufacturer's software (Antera 3D CS, version 3.1.16) within a circular ROI of 21 mm diameter placed at the same position on each image. Erythema maps were reconstructed from the multispectral data and characterized by the Redness Score together with its minimum, maximum and uniformity values within the ROI, describing the intensity and spatial distribution of the hemoglobin-related optical signal, which is an indirect measure of the superficial vascular component. All measurements were performed according to the manufacturer's recommendations and used for the quantitative assessment of changes during therapy.

2.9. Measurement Reliability and Quality Control

All imaging examinations were performed in the same laboratory room, under the environmental conditions described above, by the same two trained investigators, and the follow-up examinations were scheduled at a similar time of day as the baseline examination whenever possible. For each modality, a single acquisition per thigh and time point was used for analysis. Image quality was checked immediately after acquisition, and the acquisition was repeated if the image was technically inadequate (motion artifacts, incomplete coverage of the ROI, incorrect focus or saturation); the repeated image replaced the inadequate one, and no further selection of images was performed. No image or participant was excluded from the analysis, and no measurement was missing at any time point. ROI placement was performed by a single investigator for each modality, and all

parameters were computed automatically within the ROIs using identical software settings. A formal assessment of the intra- and inter-observer reproducibility of ROI placement and of the test–retest repeatability of the imaging parameters was not performed in the present study, and the investigators who processed the images were not blinded to the time point of acquisition; both issues are acknowledged as limitations in Section 4. Consequently, the measurement error of the individual parameters, and hence the smallest change that can be distinguished from measurement noise, is not known for the present set-up. The results are therefore reported as group-level longitudinal changes, and no attempt was made to classify individual participants as responders or non-responders.

2.10. Statistical Analysis

The distribution of the variables was assessed before selecting the analytical methods. Comparisons between the three time points (T1, T2 and T3) were performed with the Friedman test, followed by Dunn's post hoc test when significant differences were found; a Bonferroni adjustment was applied to the three pairwise comparisons between measurement time points. Paired comparisons between two dependent measurements used the Wilcoxon signed-rank test. Correlations between the imaging parameters and the clinical grading were not analyzed. A value of $p < 0.05$ was considered statistically significant. The left and right thighs were analyzed separately and were not treated as independent observations within a pooled analysis. For each side-specific longitudinal analysis, the statistical unit was the participant ($n = 30$), with repeated measurements obtained from the same thigh at T1, T2, and T3. The Friedman test accounted for the repeated-measures structure across time within each thigh. The within-participant correlation between the left and right thighs was not explicitly modeled. No additional adjustment for multiple testing was applied across the different imaging parameters or modalities. Accordingly, the analyses were considered exploratory, and the reported P-values should be interpreted with caution. Results are presented as mean ± standard deviation (SD) or as median with interquartile range (IQR), depending on the distribution of the variable; effect sizes are reported as Kendall's W (and as r for the Wilcoxon test), interpreted as small (about 0.1), moderate (about 0.3) or large (0.5 or more) [17]. Because of the number of parameters analyzed, the consistency of the direction of change across modalities and the magnitude of the effect sizes were given more weight in the interpretation than individual *p*-values. For the main longitudinal comparison (T1 vs. T3), the median of the paired differences with its 95% confidence interval (Hodges–Lehmann estimate) and the Wilcoxon effect size r are additionally reported for each parameter in Supplementary Table S1. No formal hypothesis hierarchy was tested; the results are presented as descriptive estimates of treatment-associated change over time and not as tests of treatment efficacy.

3. Results

3.1. Clinical Photography (GLCM)

Quantitative analysis of clinical photographs showed a progressive change in skin-surface texture parameters during treatment (Figure 2), reflected by a decrease in GLCM Contrast and a corresponding increase in GLCM Homogeneity, compatible with gradual smoothing of the skin surface.

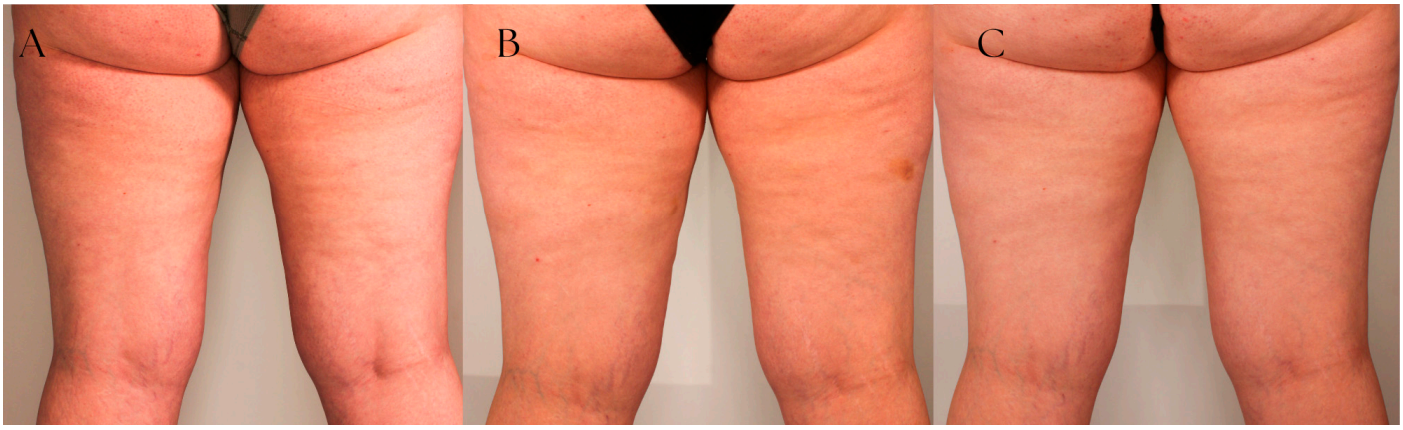


Figure 2. Representative standardized cross-polarized photographs of the posterior thighs of one participant with cellulite during ALIDYA treatment: (A) baseline (T1), (B) intermediate assessment (T2), and (C) final follow-up (T3). Images illustrate the change in skin-surface regularity and the attenuation of visible cellulite-related irregularities over the treatment period. All three panels were acquired with the same standardized Fotomedicus setup and were cropped to the same anatomical landmarks (gluteal fold and popliteal crease) at identical magnification; color balance was not altered.

3.1.1. GLCM Contrast

A significant time effect was found for GLCM Contrast in the left thigh ($p < 0.001$, Kendall's W = 0.25) and the right thigh ($p = 0.001$, Kendall's W = 0.22) (Table 1; Figure 3). Post-hoc analysis showed significant T1–T2 and T1–T3 differences for the left thigh ($p = 0.014$ and $p < 0.001$, respectively), whereas for the right thigh, significance was observed only between T1 and T3 ($p < 0.001$).

Table 1. Changes in Gray-Level Co-occurrence Matrix (GLCM) Contrast derived from standardized cross-polarized photographs of the left and right thighs during ALIDYA treatment. Measurements were performed at baseline (T1), at the intermediate assessment (T2), and at the final follow-up (T3). Data are presented as median (Q1–Q3). Statistical significance was assessed using the Friedman test followed by Dunn's post hoc test with Bonferroni adjustment. Effect size is expressed as Kendall's W.

Thigh	Time	Median (Q1–Q3)	*p*-Value	Effect Size	Post hoc T1	Post hoc T2	Post hoc T3
Left	T1	1.414 (1.141–1.690)	<0.001	0.25	–	0.014	<0.001
	T2	1.379 (0.963–1.596)			0.014	–	1.000
	T3	1.288 (1.009–1.479)			<0.001	1.000	–
Right	T1	1.385 (1.123–1.642)	0.001	0.22	–	0.212	<0.001
	T2	1.371 (1.074–1.559)			0.212	–	0.212
	T3	1.246 (1.000–1.448)			<0.001	0.212	–

3.1.2. GLCM Homogeneity

A significant time effect was also found for GLCM Homogeneity in the left thigh ($p = 0.002$, Kendall's W = 0.20) and the right thigh ($p < 0.001$, Kendall's W = 0.36) (Table 2; Figure 3). Post-hoc analysis showed a significant T1–T3 difference for the left thigh ($p = 0.001$), whereas for the right thigh, significant differences were observed between T1 and T2 ($p = 0.004$) and between T1 and T3 ($p < 0.001$).

Table 2. Changes in Gray-Level Co-occurrence Matrix (GLCM) Homogeneity derived from standardized cross-polarized photographs of the left and right thighs during ALIDYA treatment. Measurements were performed at baseline (T1), at the intermediate assessment (T2), and at the final follow-up (T3). Data are presented as median (Q1–Q3). Statistical significance was assessed using the Friedman test followed by Dunn's post hoc test with Bonferroni adjustment. Effect size is expressed as Kendall's W.

Thigh	Time	Median (Q1–Q3)	*p*-Value	Effect Size	Post hoc T1	Post hoc T2	Post hoc T3
Left	T1	0.707 (0.671–0.733)	0.002	0.20	–	0.364	0.001
	T2	0.702 (0.683–0.741)			0.364	–	0.158
	T3	0.728 (0.700–0.769)			0.001	0.158	–
Right	T1	0.699 (0.673–0.726)	<0.001	0.36	–	0.004	<0.001
	T2	0.713 (0.690–0.741)			0.004	–	0.590
	T3	0.730 (0.693–0.762)			<0.001	0.590	–

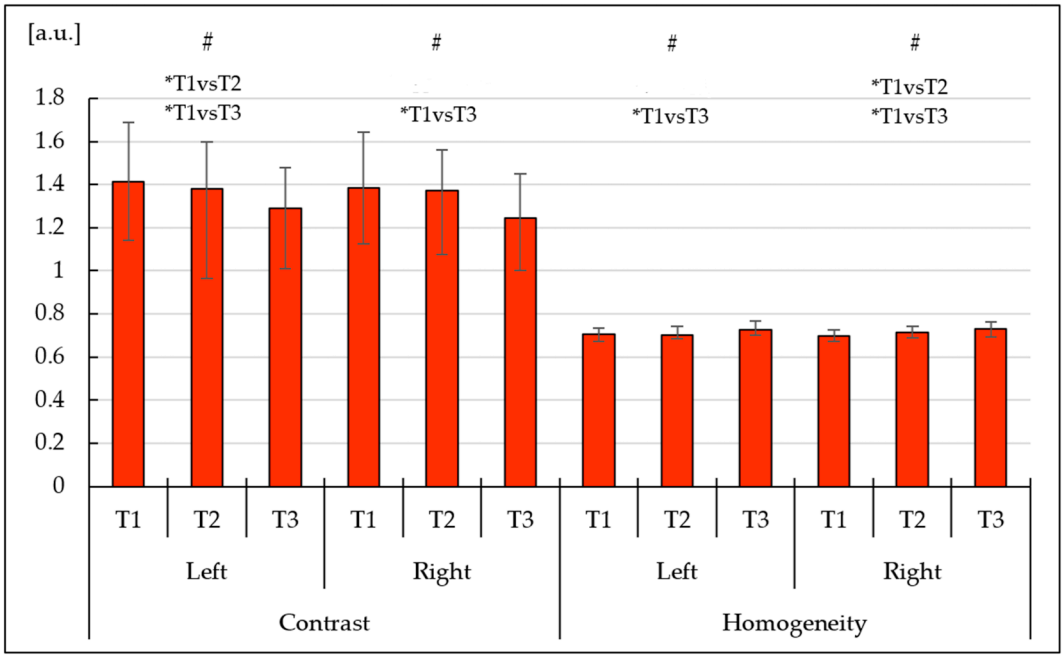


Figure 3. Changes in Gray-Level Co-occurrence Matrix (GLCM) Contrast and Homogeneity derived from standardized cross-polarized photographs of the left and right thighs during ALIDYA treatment. Measurements were performed at baseline (T1), at the intermediate assessment (T2), and at the final follow-up (T3). Bars represent medians, and whiskers indicate the first and third quartiles (Q1–Q3). a.u. – arbitrary units. # indicates a statistically significant overall time effect (Friedman test, $p < 0.05$; exact P-values and effect sizes are given in Tables 1 and 2). Asterisks indicate statistically significant pairwise differences according to Dunn's post hoc test with Bonferroni adjustment (* $p < 0.05$).

3.2. Thermography

Thermographic texture analysis demonstrated progressive changes in the spatial distribution of skin temperature throughout the treatment period. A reduction in thermal heterogeneity was observed over the treatment period, i.e., a more uniform spatial distribution of skin surface temperature within the treated area (Figure 4).

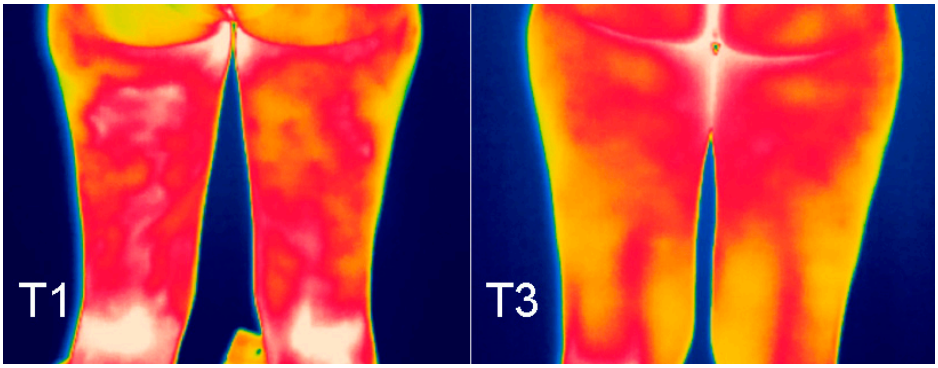


Figure 4. Representative thermograms of the posterior thighs of one participant with cellulite at baseline (T1) and the final follow-up (T3), acquired under identical environmental conditions and displayed with the same temperature scale. The mosaic pattern of warmer and cooler areas visible at baseline becomes more uniform at T3.

3.2.1. Thermographic Contrast

Thermographic GLCM Contrast decreased over time in both thighs, with significant overall differences for the left (p = 0.003, Kendall's W = 0.19) and right thigh (p = 0.001, Kendall's W = 0.22) (Table 3; Figure 5). Post-hoc analysis showed a significant decrease between T1 and T3 for both the left (p = 0.002) and right thigh (p < 0.001).

Table 3. Changes in Gray-Level Co-occurrence Matrix (GLCM) Contrast derived from thermographic images of the left and right thighs during ALIDYA treatment. Measurements were performed at baseline (T1), at the intermediate assessment (T2), and at the final follow-up (T3). Data are presented as medians (Q1–Q3). Statistical significance was assessed using the Friedman test followed by Dunn's post hoc test with Bonferroni adjustment. Effect size is expressed as Kendall's W.

Thigh	Time	Median (Q1–Q3)	*p*-Value	Effect Size	Post hoc T1	Post hoc T2	Post hoc T3
Left	T1	0.615 (0.461–0.725)	0.003	0.19	–	0.590	0.002
	T2	0.623 (0.441–0.737)			0.590	–	0.117
	T3	0.565 (0.403–0.715)			0.002	0.117	–
Right	T1	0.657 (0.506–0.769)	0.001	0.22	–	0.212	<0.001
	T2	0.668 (0.471–0.779)			0.212	–	0.212
	T3	0.625 (0.423–0.748)			<0.001	0.212	–

3.2.2. Thermographic Homogeneity

Thermographic GLCM Homogeneity increased over time in both thighs, with significant overall differences for the left (p = 0.012, Kendall's W = 0.15) and right thigh (p < 0.001, Kendall's W = 0.34) (Table 4; Figure 5). Post-hoc analysis showed a significant increase between T1 and T3 for the left thigh (p = 0.011), while for the right thigh, significant increases were found between T1 and T3 (p < 0.001) and between T2 and T3 (p = 0.020).

Table 4. Changes in Gray-Level Co-occurrence Matrix (GLCM) Homogeneity derived from thermographic images of the left and right thighs during ALIDYA treatment. Measurements were performed at baseline (T1), at the intermediate assessment (T2), and at the final follow-up (T3). Data are presented as medians (Q1–Q3). Statistical significance was assessed using the Friedman test followed by Dunn's post hoc test with Bonferroni adjustment. Effect size is expressed as Kendall's W.

Thigh	Time	Median (Q1–Q3)	*p*-Value	Effect Size	Post hoc T1	Post hoc T2	Post hoc T3
Left	T1	0.842 (0.819–0.856)	0.012	0.15	–	0.999	0.011
	T2	0.837 (0.820–0.864)			0.999	–	0.158

	T3	0.850 (0.830–0.876)			0.011	0.158	–
Right	T1	0.832 (0.816–0.847)	<0.001	0.34	–	0.244	<0.001
	T2	0.838 (0.809–0.859)			0.244	–	0.020
	T3	0.847 (0.807–0.874)			<0.001	0.020	–

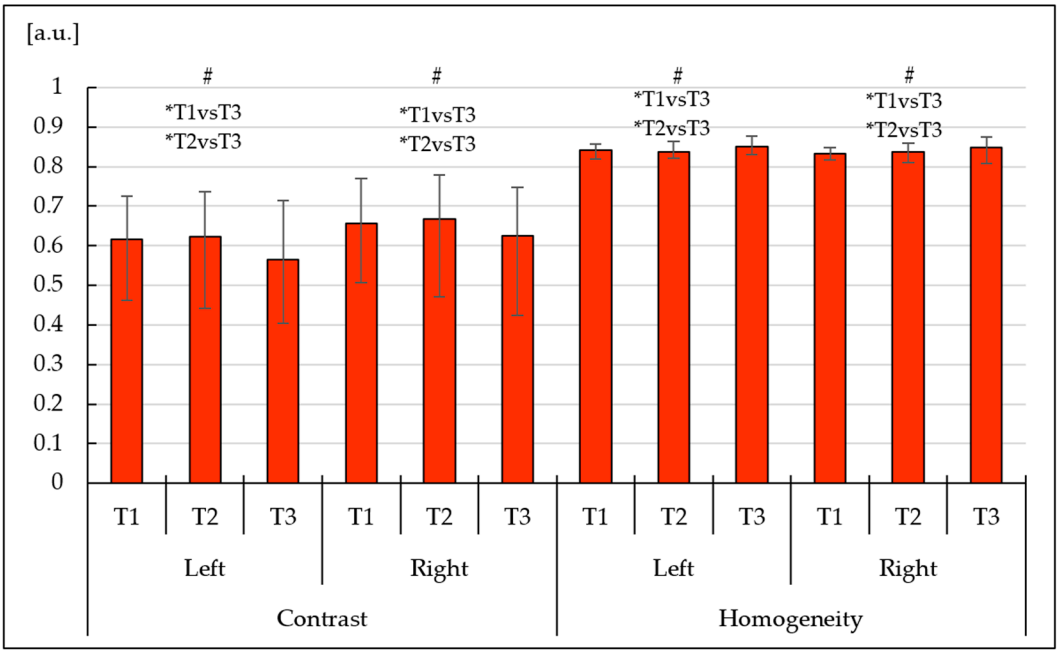


Figure 5. Changes in Gray-Level Co-occurrence Matrix (GLCM) Contrast and Homogeneity derived from thermographic images of the left and right thighs during ALIDYA treatment. Measurements were performed at baseline (T1), at the intermediate assessment (T2), and at the final follow-up (T3). Bars represent medians, and whiskers indicate the first and third quartiles (Q1–Q3). a.u. – arbitrary units. # indicates a statistically significant overall time effect (Friedman test, $p < 0.05$; exact P-values and effect sizes are given in Tables 3 and 4). Asterisks indicate statistically significant pairwise differences according to Dunn's post hoc test with Bonferroni adjustment (* $p < 0.05$).

3.3. Hyperspectral Imaging

Hyperspectral imaging revealed changes in the hemoglobin-related spectral indices and in the VIS slope over the treatment period, whereas the water-related index and the NIR slope did not change significantly.

3.3.1. Hemoglobin-Related Indices

HbDepth560 decreased over time ($p = 0.002$, Kendall's W = 0.20), whereas R560/R650 and R577/R650 increased (both $p < 0.001$; Kendall's W = 0.31 and 0.29, respectively) (Table 5; Figure 6). Significant differences were found between T1 and T2 (HbDepth560: $p = 0.043$; R560/R650: $p = 0.002$; R577/R650: $p = 0.009$) and between T1 and T3 (HbDepth560: $p = 0.002$; R560/R650 and R577/R650: both $p < 0.001$).

Table 5. Changes in hemoglobin-related hyperspectral imaging indices (HbDepth560, R560/R650, and R577/R650) during ALIDYA treatment. Measurements were performed at baseline (T1), at the intermediate assessment (T2), and at the final follow-up (T3). Data are presented as medians (Q1–Q3). Statistical significance was assessed using the Friedman test followed by Dunn's post hoc test with Bonferroni adjustment. Effect size is expressed as Kendall's W.

Parameter	Time	Median (Q1–Q3)	*p*-Value	Effect Size	Post hoc T1	Post hoc T2	Post hoc T3
HbDepth560	T1	0.128 (0.086–0.177)	0.002	0.20	–	0.043	0.002
	T2	0.086 (0.055–0.142)			0.043	–	1.000
	T3	0.090 (0.034–0.140)			0.002	1.000	–
R560/R650	T1	0.496 (0.473–0.518)	<0.001	0.31	–	0.002	<0.001
	T2	0.529 (0.485–0.552)			0.002	–	1.000
	T3	0.529 (0.486–0.583)			<0.001	1.000	–
R577/R650	T1	0.525 (0.500–0.551)	<0.001	0.29	–	0.009	<0.001
	T2	0.553 (0.508–0.576)			0.009	–	0.905
	T3	0.549 (0.500–0.607)			<0.001	0.905	–

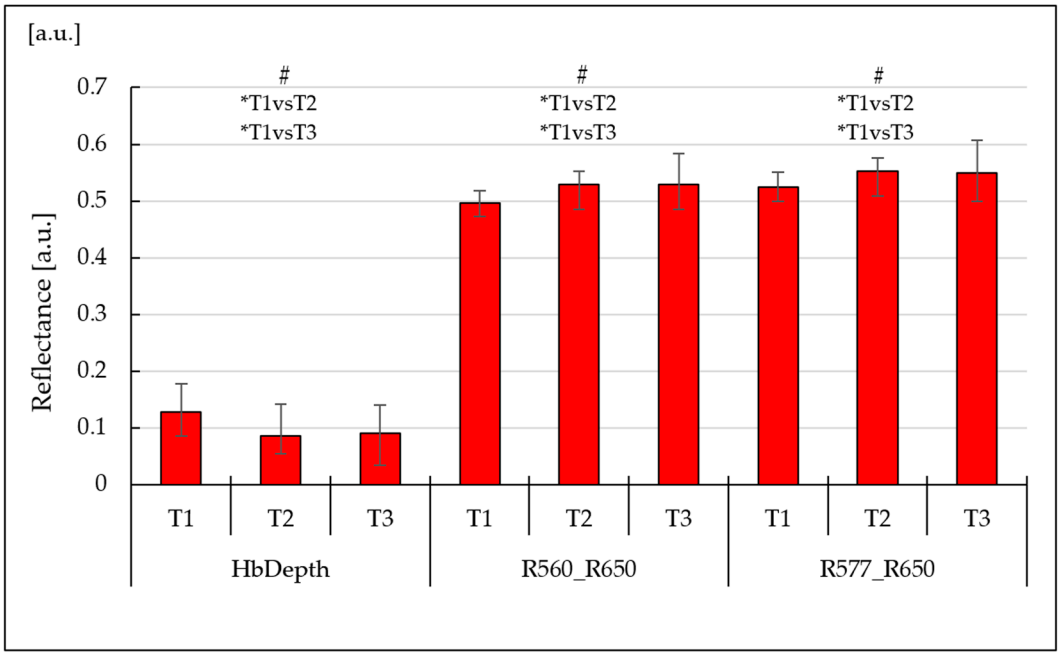


Figure 6. Changes in hemoglobin-related hyperspectral imaging indices (HbDepth560, R560/R650 and R577/R650) during ALIDYA treatment. Measurements were performed at baseline (T1), at the intermediate assessment (T2), and at the final follow-up (T3). Bars represent medians, and whiskers indicate the first and third quartiles (Q1–Q3). a.u. – arbitrary units. # indicates a statistically significant overall time effect (Friedman test, $p < 0.05$; exact P-values and effect sizes are given in Table 5). Asterisks indicate statistically significant pairwise differences according to Dunn's post hoc test with Bonferroni adjustment (* $p < 0.05$).

3.3.2. Water-Related Index

Water970_800 showed a slight increase over time, but the overall difference was not significant ($p = 0.967$, Kendall's W = 0.00) (Table 6).

Table 6. Changes in the water-related hyperspectral imaging index (Water970_800) during ALIDYA treatment. Measurements were performed at baseline (T1), at the intermediate assessment (T2), and at the final follow-up (T3). Data are presented as medians (Q1–Q3). Statistical significance was assessed using the Friedman test followed by Dunn's post hoc test with Bonferroni adjustment. Effect size is expressed as Kendall's W.

Parameter	Time	Median (Q1–Q3)	*p*-Value	Effect Size	Post hoc T1	Post hoc T2	Post hoc T3
Water970_800	T1	0.887 (0.874–0.914)	0.967	0.00	–	1.000	1.000
	T2	0.891 (0.864–0.919)			1.000	–	1.000
	T3	0.895 (0.875–0.918)			1.000	1.000	–

3.3.3. Reflectance Slope Parameters

VIS slope increased over time ($p = 0.016$, Kendall's W = 0.14), with a significant difference between T1 and T3 ($p = 0.014$) (Table 7). NIR slope showed a slight increase, but the overall difference was not significant ($p = 0.792$, Kendall's W = 0.01).

Table 7. Changes in hyperspectral imaging reflectance parameters (VIS slope and NIR slope) during ALIDYA treatment. Measurements were performed at baseline (T1), at the intermediate assessment (T2), and at the final follow-up (T3). Data are presented as medians (Q1–Q3). Statistical significance was assessed using the Friedman test followed by Dunn's post hoc test with Bonferroni adjustment. Effect size is expressed as Kendall's W.

Parameter	Time	Median (Q1–Q3)	*p*-Value	Effect Size	Post hoc T1	Post hoc T2	Post hoc T3
VIS slope 500–600 nm	T1	0.00035 (0.00027–0.00044)	0.016	0.14	–	0.905	0.014
	T2	0.00038 (0.00032–0.00045)			0.905	–	0.212
	T3	0.00043 (0.00032–0.00051)			0.014	0.212	–
NIR slope 700–900 nm	T1	0.00018 (0.00012–0.00027)	0.792	0.01	–	1.000	1.000
	T2	0.00019 (0.00012–0.00027)			1.000	–	1.000
	T3	0.00022 (0.00014–0.00025)			1.000	1.000	–

3.4. Antera 3D Erythema

Multispectral analysis with the Antera 3D system showed a progressive decrease in the erythema parameters (Redness Score and its minimum and maximum values) over the treatment period, whereas the Uniformity index did not change.

Redness Score decreased over time in both the left and right thighs (both $p < 0.001$; Kendall's W = 0.54 and 0.46, respectively) (Table 8; Figures 7 and 8). Significant decreases were observed between T1 and T2 and between T1 and T3 for both thighs (left: $p = 0.020$ and $p < 0.001$; right: $p = 0.002$ and $p < 0.001$, respectively), with an additional significant decrease between T2 and T3 in the left thigh ($p = 0.011$).

Minimum values also decreased in both thighs (both $p < 0.001$; Kendall's W = 0.49 for the left and 0.32 for the right thigh). Significant decreases were observed between T1 and T2 and between T1 and T3 for both thighs (left: both $p < 0.001$; right: $p = 0.006$ and $p < 0.001$, respectively).

Maximum values decreased in both thighs (both $p < 0.001$; Kendall's W = 0.55 for the left and 0.37 for the right thigh). Significant decreases were observed between T1 and T2 and between T1 and T3 for both thighs (all $p < 0.001$).

Uniformity showed no significant changes over time in either the left ($p = 0.149$, Kendall's W = 0.06) or right thigh ($p = 0.356$, Kendall's W = 0.03).

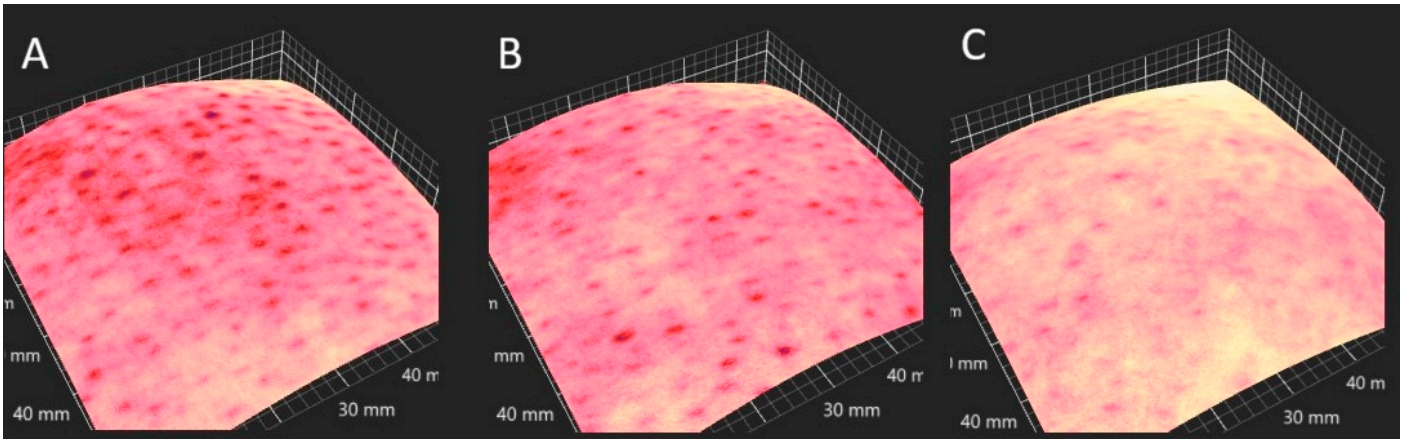


Figure 7. Example of change in the severity of erythema measured by Antera 3D on the right thigh: (A) baseline (T1), (B) intermediate assessment (T2) and (C) final follow-up (T3). Both images were acquired at the same position of the measurement head and are displayed with the same color scale.

Table 8. Changes in Antera 3D-derived erythema parameters (Redness Score, Minimum, Maximum, and Uniformity) of the left and right thighs during ALIDYA treatment. Measurements were performed at baseline (T1), at the intermediate assessment (T2), and at the final follow-up (T3). Data are presented as medians (Q1–Q3). Statistical significance was assessed using the Friedman test followed by Dunn's post hoc test with Bonferroni adjustment. Effect size is expressed as Kendall's W.

Parameter	Thigh	Time	Median (Q1–Q3)	*p*-Value	Effect Size	Post hoc T1	Post hoc T2	Post hoc T3
Redness Score	Left	T1	37.00 (34.00–41.50)	<0.001	0.54	–	0.020	<0.001
		T2	32.50 (28.00–36.50)			0.020	–	0.011
		T3	32.25 (26.00–35.50)			<0.001	0.011	–
	Right	T1	37.00 (34.50–41.00)	<0.001	0.46	–	0.002	<0.001
		T2	33.00 (31.00–36.00)			0.002	–	0.320
		T3	33.00 (30.00–35.50)			<0.001	0.320	–
Minimum	Left	T1	13.28 (12.59–14.66)	<0.001	0.49	–	<0.001	<0.001
		T2	12.63 (12.06–14.05)			<0.001	–	0.320
		T3	12.46 (11.80–14.05)			<0.001	0.320	–
	Right	T1	14.80 (13.45–16.16)	<0.001	0.32	–	0.006	<0.001
		T2	13.69 (12.41–15.55)			0.006	–	0.736
		T3	13.40 (12.37–15.05)			<0.001	0.736	–
Maximum	Left	T1	29.90 (26.35–33.63)	<0.001	0.55	–	<0.001	<0.001
		T2	24.64 (21.30–31.71)			<0.001	–	0.467
		T3	23.90 (20.86–32.68)			<0.001	0.467	–
	Right	T1	31.57 (26.52–36.76)	<0.001	0.37	–	<0.001	<0.001
		T2	27.42 (23.69–33.45)			<0.001	–	1.000
		T3	27.40 (23.75–32.78)			<0.001	1.000	–
Uniformity	Left	T1	37.71 (30.19–43.26)	0.149	0.06	–	0.158	0.736
		T2	39.17 (31.61–42.09)			0.158	–	1.000
		T3	38.63 (31.18–43.74)			0.736	1.000	–
	Right	T1	47.08 (43.63–52.07)	0.356	0.03	–	1.000	0.467
		T2	48.59 (42.20–52.42)			1.000	–	1.000
		T3	48.31 (41.43–51.94)			0.467	1.000	–

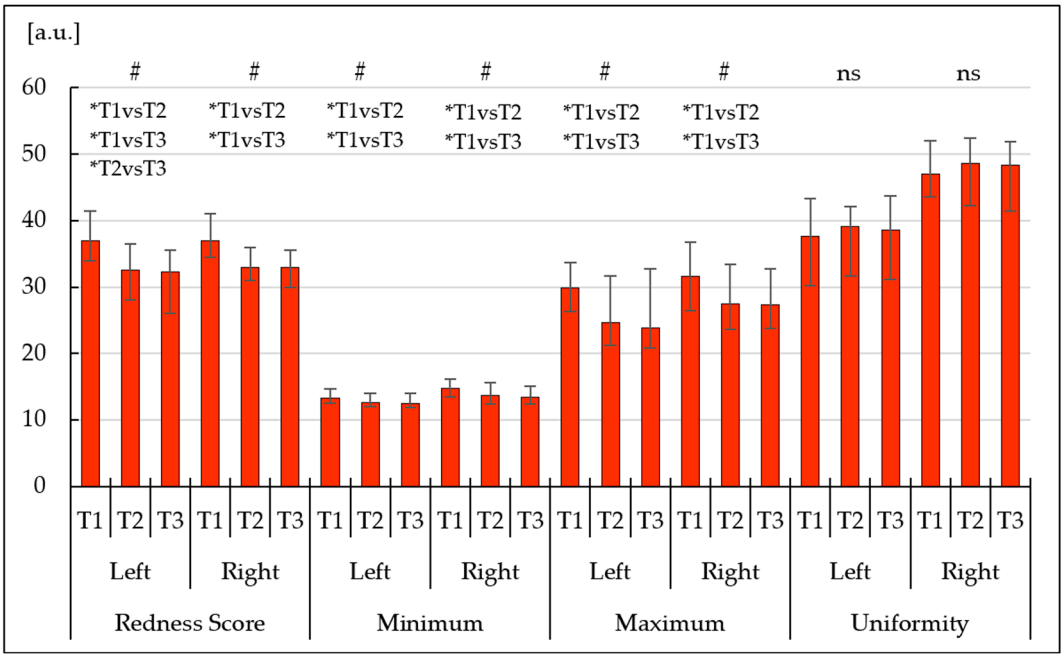


Figure 8. Changes in Antera 3D-derived erythema parameters (Redness Score, Minimum, Maximum, and Uniformity) of the left and right thighs during ALIDYA treatment. Measurements were performed at baseline (T1), at the intermediate assessment (T2), and at the final follow-up (T3). Bars represent medians, and whiskers indicate the first and third quartiles (Q1–Q3). a.u. – arbitrary units. # indicates a statistically significant overall time effect (Friedman test, $p < 0.05$; exact P-values and effect sizes are given in Table 8); ns, not significant. Asterisks indicate statistically significant pairwise differences according to Dunn's post hoc test with Bonferroni adjustment (* $p < 0.05$).

3.5. Safety and Tolerability

All 30 participants completed the six treatment sessions and all three assessments. The treatment was well tolerated. The only adverse events were bruising at the injection sites, accompanied by local tenderness, which occurred in 8 of 30 participants (26.7%) after one or more sessions and resolved spontaneously within 7–14 days without treatment. Transient erythema at the injection points immediately after the procedure, which is expected after needle mesotherapy, resolved within a few hours. No infection, hematoma requiring intervention, allergic reaction, skin necrosis, post-inflammatory pigmentary change or systemic adverse event was observed. No participant required medical intervention, a change in the treatment protocol or discontinuation of treatment because of an adverse event.

4. Discussion

Assessment of the efficacy of anti-cellulite therapy should extend beyond subjective clinical grading to include objective parameters capable of quantifying its microvascular component, which, as outlined in the Introduction, is one of the key elements of cellulite pathophysiology [1,3]. The present exploratory study addressed this need by integrating four complementary imaging modalities into a single prospective evaluation protocol applied before, during and after a series of ALIDYA treatments.

One of the main findings is the concordant direction of change across the imaging techniques: photographic texture parameters, thermographic texture parameters, hemoglobin-related hyperspectral indices and Antera 3D erythema parameters all changed over the treatment period in a direction compatible with a reduction in the microvascular disturbance characteristic of cellulite. Because each modality relies on a different physical principle (surface topography, emitted infrared radiation, reflectance spectroscopy and

multispectral separation of chromophores), this convergence makes a modality-specific artifact an unlikely explanation of the results. It does not, however, demonstrate improved cutaneous perfusion. None of the methods used measures blood flow directly, and in the absence of a control group the observed changes cannot be attributed with certainty to the treatment itself. Throughout this Discussion we therefore speak of changes observed during the treatment period and distinguish them from effects specifically attributable to the ALIDYA formulation.

Conventional grading systems remain the reference standard in clinical practice, but they are observer-dependent and insufficiently responsive to the subtle changes occurring during treatment [1,2]. In the present study, most, though not all, of the imaging parameters changed significantly over the three-month observation period. The GLCM parameters of photographs and thermograms, the hemoglobin-related hyperspectral indices, the VIS slope and the Antera 3D Redness Score with its minimum and maximum values showed significant changes, whereas the water-related index Water970_800 ($p = 0.967$), the NIR slope ($p = 0.792$) and the Antera 3D Uniformity index ($p = 0.149$ and $p = 0.356$ for the left and right thigh, respectively) did not. Moreover, several pairwise comparisons between baseline and the intermediate assessment did not reach significance, particularly for the right thigh, so that an early change at T2 can be claimed only for some parameters. Instrumental imaging therefore appears sensitive enough to detect treatment-associated changes, but the pattern of results is not uniform across parameters, and this heterogeneity should be borne in mind when interpreting the findings. Given the number of parameters tested without a global adjustment for multiplicity, we attach more importance to the consistency of the direction of change across modalities and to the effect sizes than to any individual P-value; the median paired changes between T1 and T3 with their 95% confidence intervals are listed in Supplementary Table S1.

Digital image analysis using GLCM algorithms demonstrated reduced contrast together with increased homogeneity of the skin surface, indicating progressive smoothing of tissue topography. In cellulite, elevated contrast reflects abrupt transitions between protruding adipose lobules and tethered skin depressions, whereas increasing homogeneity corresponds to restoration of a smoother, more continuous surface [6,16]. Because these surface irregularities are amplified by interstitial edema and by locally heterogeneous perfusion, their attenuation is compatible with a reduction in interstitial edema and in heterogeneous perfusion, although texture parameters alone cannot distinguish between vascular, interstitial and structural causes of surface smoothing [3,6].

The thermographic findings provide complementary information on the thermal consequences of the microvascular disturbance. Disturbances of venous return, lymphatic drainage and capillary perfusion are fundamental components of cellulite pathophysiology and produce the heterogeneous “leopard-skin” thermal pattern [2,4]. Rather than relying on average skin temperature, which has limited diagnostic value, we analyzed thermographic texture using GLCM-derived descriptors, demonstrating significant increases in thermal homogeneity, i.e., a more uniform spatial distribution of skin surface temperature. Such a change is compatible with, but does not demonstrate, a more uniform distribution of superficial blood flow. Skin surface temperature is, however, an indirect indicator of perfusion that is also influenced by the thickness of the subcutaneous tissue, ambient conditions and vasomotor tone, and these changes cannot be equated with a normalization of vascular function. Previous instrumental studies similarly identified thermographic texture analysis as a sensitive objective marker of treatment-related change in cellulite [6,16].

Hyperspectral imaging provided perhaps the most informative findings from the biological point of view, although their interpretation remains indirect. Unlike conventional RGB photography, hyperspectral systems record continuous reflectance spectra for every

pixel, allowing for simultaneous assessment of multiple tissue chromophores. The physical meaning of the three hemoglobin-related indices deserves comment, because it determines what can and cannot be inferred from them. HbDepth560 quantifies the depth of the absorption feature centered near 560 nm relative to a baseline fitted between 510 and 610 nm. This spectral region is dominated by the absorption bands of oxyhemoglobin (542 and 577 nm) and deoxyhemoglobin (556 nm), so that the depth of the feature increases with the amount of hemoglobin within the sampling volume, while the baseline correction partly removes the slowly varying contributions of scattering and melanin. R560/R650 and R577/R650 relate the reflectance at the hemoglobin bands to the reflectance at 650 nm, where hemoglobin absorbs weakly; an increase in these ratios means that less light is absorbed at the hemoglobin bands relative to the reference wavelength. The three indices thus changed in a mutually consistent manner (a shallower absorption feature and higher ratios), and the most parsimonious explanation is a decrease in the hemoglobin-related absorption of the superficial dermis within the sampling depth of visible light, which is of the order of 0.5–1 mm. A change in oxygenation would primarily alter the shape of the feature, since the 542 and 577 nm bands of oxyhemoglobin and the 556 nm band of deoxyhemoglobin would change in opposite directions, and R577/R650 would then be expected to change more than R560/R650; this was not observed, but with the indices used here, a change in oxygenation cannot be separated from a change in concentration. Two further factors must be considered. First, all three indices are also sensitive to tissue scattering: a change in scattering, for example as a consequence of altered interstitial fluid content or ECM remodeling, modifies the overall reflectance and the slope of the spectrum, and the concomitant increase in the VIS slope indicates that the optical properties of the tissue changed in the 500–600 nm range beyond hemoglobin absorption alone. Second, the 650 nm reference is affected by melanin, so that a change in pigmentation over the three-month study period could in principle contribute to the ratios, although it would not explain the change in the baseline-corrected HbDepth560. What can reasonably be inferred from the spectral data is therefore a decrease in hemoglobin-related absorption in the superficial dermis accompanied by a change in tissue scattering; what cannot be inferred is whether this reflects reduced vessel dilatation, reduced vessel density, altered oxygenation or a redistribution of blood to deeper layers.

The unchanged Water970_800 index must be interpreted with equal caution and should not be taken as evidence that the interstitial fluid content did not change. The water absorption band at 970 nm is weak compared with the bands at 1200 and 1450 nm, which lie outside the spectral range of the camera; the quantum efficiency of the silicon detector decreases markedly toward 1000 nm, which lowers the signal-to-noise ratio in this region; and light at 800–970 nm samples a depth of several millimeters, so that the index averages the water content of the dermis and the upper subcutaneous tissue and is relatively insensitive to a modest change in dermal interstitial fluid. The absence of a significant change in this index therefore indicates only that any change in tissue water was below the sensitivity of the method, and it does not exclude a reduction in interstitial edema, which remains an important element of current concepts of cellulite alongside ECM remodeling, fibrosis, chronic microvascular dysfunction and oxidative stress [3,5,18]. The hemoglobin-related changes should accordingly be interpreted on their own merits, without inferring from the water index that edema remained unchanged.

This interpretation is consistent with prior optical investigations demonstrating that diffuse reflectance spectroscopy enables quantitative assessment of hemoglobin concentration, melanin content and tissue scattering [10,12,13,19], and with recent advances establishing pixel-wise spectral analysis as a highly sensitive method for evaluating subtle physiological changes in the skin [14,20,21]. The changes in spectral indices observed during the treatment period may therefore reflect an altered distribution of superficial

hemoglobin and altered tissue optical properties, but the underlying mechanism cannot be established from reflectance data alone. As relatively few studies have applied hyperspectral imaging to cellulite, this aspect of the present work is particularly novel.

Antera 3D erythema analysis provided an independent, spatially resolved assessment of superficial erythema. Multispectral separation of hemoglobin from the remaining chromophores allows erythema to be quantified without the confounding influence of surface reflection or pigmentation [15], and the significant reduction in Redness Score together with its minimum and maximum values is compatible with a decrease in the hemoglobin-related optical signal from the papillary dermis across the whole treated field. The stability of the erythema uniformity index suggests a generalized decrease in the intensity of the vascular component rather than the disappearance of isolated hyperemic foci. Because Antera 3D, thermography and hyperspectral imaging derive their signals from different physical phenomena, their concordance argues against a modality-specific artifact, although it does not by itself establish an improvement of the cutaneous microcirculation.

The decrease in the erythema parameters requires particularly cautious interpretation. The Redness Score quantifies the optical signal attributable to superficial hemoglobin; it does not measure blood flow, vessel density or inflammatory activity, none of which was assessed in this study. Reduced redness may result from a decrease in vessel dilatation or density, from a change in hemoglobin oxygenation or from fluctuations in vasomotor tone related to ambient temperature or to the emotional state of the participant. Residual bruising after earlier injection sessions could in principle also have affected the signal at the intermediate assessment in some participants, although such an effect would be expected to increase rather than decrease the measured redness. We therefore report the decrease in the erythema parameters as a treatment-associated optical change compatible with an alteration of the superficial vascular component, and not as evidence of reduced inflammation or improved perfusion.

It should also be kept in mind that the intervention comprised two components that cannot be separated in a single-arm design: the ALIDYA formulation and the repeated needle penetration of the dermis. Needling alone induces a wound-healing response with transient vasodilatation, release of growth factors and subsequent remodeling of the dermal matrix, and six sessions of microinjections distributed over the whole posterior thigh may therefore modify the texture, thermal and optical parameters independently of the injected product. Physiological variability, including the phase of the menstrual cycle, ambient temperature and seasonal changes in cutaneous blood flow over the three-month observation period, adds further variance that a single-arm design cannot control. For these reasons the changes described here are attributed to the treatment period as a whole, and no inference is drawn about the EDTA-related mechanism proposed for the product.

The clinical relevance of the observed changes is a separate question from their statistical significance, and the two should not be conflated. In terms of magnitude, the median photographic GLCM Contrast was 9–10% lower and Homogeneity 3–4% higher at T3 than at T1; thermographic Contrast was 5–8% lower and Homogeneity 1–2% higher; HbDepth560 was about 30% lower, whereas the reflectance ratios were 5–7% higher; and the Antera 3D Redness Score was 11–13% lower, with a 13–20% decrease in its maximum value. The effect sizes followed the same ranking: Kendall's W was moderate to large for the Antera 3D erythema parameters (0.32–0.55), moderate for the hemoglobin-related hyperspectral indices (0.20–0.31) and the photographic texture parameters (0.20–0.36), small to moderate for the thermographic texture parameters (0.15–0.34) and small for the VIS slope (0.14). None of these parameters has an established minimal clinically important difference, and none has been calibrated against the clinical grading of cellulite, so that it cannot be stated whether changes of this size correspond to a difference in cellulite

severity or skin appearance that a patient or clinician would notice. Two observations are nevertheless relevant. First, the texture changes in the photographs were paralleled by visible smoothing of the skin surface in individual participants (Figure 2), which indicates that at least part of the measured change lies within the range perceptible to the eye. Second, the smallest effects (thermographic Homogeneity of the left thigh, VIS slope) are of a size that would be undetectable without quantitative analysis, and their clinical meaning, if any, remains to be determined. The relationship between the imaging parameters and the clinical grading was not analyzed, and no association between them is claimed; establishing this relationship, together with the measurement error of each parameter, is a prerequisite for defining clinically meaningful thresholds and is a priority for future work.

A methodological strength of the present investigation is the integration of complementary imaging technologies into a unified evaluation protocol; most previous cellulite studies relied on a single modality or on subjective clinical grading [16]. Simultaneous quantification of skin surface texture, thermal distribution, optical tissue composition and erythema may partly offset the limitations inherent to individual techniques and may contribute to the development of standardized candidate imaging biomarkers of the microvascular component of cellulite for future clinical trials of anti-cellulite therapies.

It should be acknowledged, however, that a multimodal protocol of this kind is resource-intensive in terms of equipment, acquisition time and analytical expertise, and in its entirety it is unlikely to be applicable in everyday ambulatory practice in the management of gynoid lipodystrophy. Its role is primarily that of a research tool for clinical trials and for the validation of simpler measures. In routine practice, single components of the protocol, for example standardized cross-polarized photography with texture analysis or a single multispectral device, could potentially be used alone, provided that their performance is first validated against the complete protocol.

The study has several limitations. First, it was a single-arm, open-label study without a placebo, sham or untreated control group. Consequently, the observed changes cannot be attributed with confidence to ALIDYA itself: natural fluctuation of cellulite severity, seasonal and environmental influences on skin temperature and blood flow, changes in physical activity or body weight during the study, regression to the mean, and the mechanical and inflammatory effects of repeated needle injections per se are all alternative explanations that could not be excluded. Second, none of the imaging modalities measures cutaneous blood flow directly. All parameters are indirect surrogate measures, and no reference method of perfusion assessment, such as laser Doppler flowmetry, laser speckle contrast imaging, color Doppler ultrasonography or capillaroscopy [22], was applied; the term “microvascular component” is therefore used throughout in the sense of a set of optical and thermal features that are influenced by, but not equivalent to, cutaneous perfusion. Third, the study was registered retrospectively (ClinicalTrials.gov, NCT07675356, first posted 30 June 2026), after the intervention had been completed. Although the imaging parameters analyzed here were registered as secondary outcomes, retrospective registration weakens the protection against selective reporting, and no imaging parameter or hierarchy of secondary endpoints was prospectively defined, so that the analyses should be considered exploratory. Fourth, no global adjustment for multiple testing was applied across the different imaging outcomes or modalities; given the exploratory nature of the analyses and the large number of parameters evaluated, the reported P-values should be interpreted with caution; for this reason the interpretation relies on the consistency of the direction of change across modalities and on the effect sizes rather than on individual P-values. Fifth, although the left and right thighs were analyzed separately, the within-participant correlation between bilateral measurements was not explicitly modeled, which is a limitation of the statistical approach. Sixth, and importantly for the intended use of these

parameters in treatment monitoring, the intra- and inter-observer reproducibility of ROI placement and the test–retest repeatability of the imaging parameters were not formally assessed under the conditions of this protocol, and the investigators who processed the images were not blinded to the time point, although all parameters were computed algorithmically within predefined ROIs. Without repeatability data, the measurement error of each parameter and the smallest detectable change are unknown, so that a change observed in an individual participant cannot be distinguished from measurement noise, and the group-level changes reported here cannot yet be translated into criteria of individual response. Reproducibility data published for the individual instruments, for example for the Antera 3D [15] or for thermographic texture analysis [6], do not replace an assessment under the conditions of the present protocol. Formal reliability testing, comprising duplicate acquisitions on the same day, independent ROI placement by two observers, intraclass correlation coefficients with confidence intervals, Bland–Altman analysis and estimation of the smallest detectable change, is therefore an essential requirement that must precede any use of these parameters as biomarkers, and it is planned as the first step of their validation. Seventh, the sample was small and consisted exclusively of women aged 20–45 years, no a priori sample-size calculation was performed, and follow-up was limited to six weeks after the last session, preventing evaluation of the long-term stability of the observed changes. Structural and clinical outcomes obtained in the same cohort, namely three-dimensional morphometry of skin depressions, high-frequency ultrasound assessment of the dermis, and clinical grading, are presented in a separate manuscript that has been submitted for publication and is currently under peer review. The present analysis and the analysis presented in that manuscript were conducted independently. Correlations between the optical or thermal parameters reported here and the structural or clinical outcomes were not examined; therefore, no relationship between these outcomes is claimed. Future randomized, sham- or placebo-controlled trials should integrate quantitative imaging with direct functional vascular measurements and molecular biomarkers, including inflammatory mediators and markers of oxidative stress, in order to clarify whether the imaging changes reported here reflect a true modification of the cutaneous microcirculation.

Despite these limitations, the present investigation shows that the period of ALIDYA treatment was associated with concordant changes in several independent, indirect imaging measures related to the cutaneous microvascular component, namely thermal homogeneity, hemoglobin-related optical indices, erythema parameters and the surface irregularity that accompanies heterogeneous perfusion. These observations are consistent with the hypothesis that the vascular component of cellulite is modifiable, a hypothesis that now requires testing in controlled studies with direct perfusion measurements; they do not identify which element of the intervention (the formulation, the repeated needle injections or both) is responsible. More broadly, the work illustrates the potential of quantitative imaging as an objective framework for evaluating aesthetic interventions and as a candidate biomarker platform that could complement subjective clinical assessment in future cellulite trials.

5. Conclusions

This prospective, single-arm, exploratory study shows that four complementary quantitative imaging techniques (cross-polarized photography with GLCM texture analysis, infrared thermography with GLCM analysis, hyperspectral imaging and Antera 3D erythema analysis) can be combined in a single protocol to monitor cellulite-associated tissue changes during an injectable treatment. During the period of six ALIDYA mesotherapy sessions, the texture, thermal, hemoglobin-related and erythema parameters changed in a concordant direction, with the largest effect sizes for the Antera 3D erythema

parameters and the hemoglobin-related hyperspectral indices, whereas the water-related index, the NIR slope and the erythema Uniformity index did not change. These parameters can be regarded as candidate imaging biomarkers of the microvascular component of cellulite for use in future studies.

The findings do not establish a specific therapeutic mechanism, do not demonstrate an improvement in cutaneous microcirculation and, in the absence of a control group, do not prove the efficacy of the product. Before the proposed parameters can be considered reliable biomarkers, their measurement reproducibility, their relationship to clinical and structural outcomes and their specificity for the vascular component must be established. Randomized controlled studies with larger cohorts, longer follow-up, prospectively registered endpoints and reference measurements of cutaneous perfusion are needed for this validation. In its full form the multimodal protocol is a research tool; validated single components of it may in future be applicable in clinical practice.

Supplementary Materials: The following supporting information can be downloaded at https://www.mdpi.com/article/10.3390/biomedicines14112434/s1, Table S1: Median paired differences between baseline (T1) and final follow-up (T3) with 95% confidence intervals (Hodges–Lehmann estimates) and Wilcoxon effect sizes (r) for all imaging parameters. Supplementary Table S2. TREND checklist. Supplementary Figure S1: Flow of Participants Through the Study.

Author Contributions: Concept, A.D. and S.W.; methodology, A.D., A.L., A.L.-T., D.W.-D. and S.W.; software and formal analysis, S.W., P.B. and M.H.-P.; research, A.D., A.L., W.O., M.G., M.W., K.M.; data analysis, A.D., W.O., M.H.-P.; writing—preparation of the first draft of the manuscript, A.D., A.L. and S.W.; writing—review and editing, all authors; visualization, S.W. and M.H.-P.; supervision, S.W. and D.W.-D.; project administration, A.D. and S.W. All authors have read and agreed to the published version of the manuscript.

Funding: This research was funded by the Medical University of Silesia in Katowice, Agreement numbers BNW-1-025/N/4/K and BNW-1-043/K/5/K.

Institutional Review Board Statement: The study was conducted in accordance with the Declaration of Helsinki and approved by the Ethics Committee of Medical University of Silesia (protocol code KNW/0022/KB1/27/I/16 and date 9 January 2024). Clinical trial registration: ClinicalTrials.gov, NCT07675356 (registered retrospectively; first posted 30 June 2026).

Informed Consent Statement: Informed consent was obtained from all subjects involved in the study. Written informed consent for publication of identifiable images has been obtained where applicable.

Data Availability Statement: The data presented in this study are available on request from the corresponding author.

Conflicts of Interest: The authors declare no conflicts of interest. The ALIDYA product used in the study was provided by the manufacturer (Marllor Biomedical, San Giovanni in Marignano, Italy), which had no role in the design of the study; in the collection, analysis or interpretation of data; in the writing of the manuscript or in the decision to publish the results.

References

1. Rossi, A.B.; Vergnanini, A.L. Cellulite: A Review. *J. Eur. Acad. Dermatol. Venereol.* **2000**, *14*, 251–262. https://doi.org/10.1046/j.1468-3083.2000.00016.x.
2. Terranova, F.; Berardesca, E.; Maibach, H. Cellulite: Nature and Aetiopathogenesis. *Int. J. Cosmet. Sci.* **2006**, *28*, 157–167. https://doi.org/10.1111/j.1467-2494.2006.00316.x.
3. Bass, L.S.; Kaminer, M.S. Insights into the Pathophysiology of Cellulite: A Review. *Dermatol. Surg.* **2020**, *46*, S77–S85. https://doi.org/10.1097/DSS.0000000000002388.

4. Lotti, T.; Ghersetich, I.; Grappone, C.; Dini, G. Proteoglycans in So-Called Cellulite. *Int. J. Dermatol.* **1990**, *29*, 272–274. https://doi.org/10.1111/j.1365-4362.1990.tb02560.x.
5. Conti, G.; Zingaretti, N.; Amuso, D.; Dai Prè, E.; Brandi, J.; Cecconi, D.; Manfredi, M.; Marengo, E.; Boschi, F.; Riccio, M.; et al. Proteomic and Ultrastructural Analysis of Cellulite-New Findings on an Old Topic. *Int. J. Mol. Sci.* **2020**, *21*, 2077. https://doi.org/10.3390/ijms21062077.
6. Wilczyński, S.; Koprowski, R.; Deda, A.; Janiczek, M.; Kuleczka, N.; Błońska-Fajfrowska, B. Thermographic Mapping of the Skin Surface in Biometric Evaluation of Cellulite Treatment Effectiveness. *Skin. Res. Technol.* **2017**, *23*, 61–69. https://doi.org/10.1111/srt.12301.
7. Hexsel, D.M.; Abreu, M.; Rodrigues, T.C.; Soirefmann, M.; do Prado, D.Z.; Gamboa, M.M.L. Side-by-Side Comparison of Areas with and without Cellulite Depressions Using Magnetic Resonance Imaging. *Dermatol. Surg.* **2009**, *35*, 1471–1477. https://doi.org/10.1111/j.1524-4725.2009.01260.x.
8. Haralick, R.M.; Shanmugam, K.S. Combined Spectral and Spatial Processing of ERTS Imagery Data. *Remote Sens. Environ.* **1974**, *3*, 3–13. https://doi.org/10.1016/0034-4257(74)90033-9.
9. Regeling, B.; Thies, B.; Gerstner, A.; Westermann, S.; Müller, N.; Bendix, J.; Laffers, W. Hyperspectral Imaging Using Flexible Endoscopy for Laryngeal Cancer Detection. *Sensors* **2016**, *16*, 1288. https://doi.org/10.3390/s16081288.
10. Zonios, G.; Bykowski, J.; Kollias, N. Skin Melanin, Hemoglobin, and Light Scattering Properties Can Be Quantitatively Assessed in Vivo Using Diffuse Reflectance Spectroscopy. *J. Investig. Dermatol.* **2001**, *117*, 1452–1457. https://doi.org/10.1046/j.0022-202x.2001.01577.x.
11. Subhash, N.; Mallia, J.R.; Thomas, S.S.; Mathews, A.; Sebastian, P.; Madhavan, J. Oral Cancer Detection Using Diffuse Reflectance Spectral Ratio R540/R575 of Oxygenated Hemoglobin Bands. *J. Biomed. Opt.* **2006**, *11*, 014018. https://doi.org/10.1117/1.2165184.
12. Yakimov, B.; Buiankin, K.; Denisenko, G.; Shitova, Y.; Shkoda, A.; Shirshin, E. Diffuse Reflectance Spectroscopy and RGB-Imaging: A Comparative Study of Non-Invasive Haemoglobin Assessment. *Sci. Rep.* **2024**, *14*, 22874. https://doi.org/10.1038/s41598-024-73084-6.
13. Nishidate, I.; Maeda, T.; Niizeki, K.; Aizu, Y. Estimation of Melanin and Hemoglobin Using Spectral Reflectance Images Reconstructed from a Digital RGB Image by the Wiener Estimation Method. *Sensors* **2013**, *13*, 7902–7915. https://doi.org/10.3390/s130607902.
14. Yudovsky, D.; Pilon, L. Retrieving Skin Properties from in Vivo Spectral Reflectance Measurements. *J. Biophotonics* **2011**, *4*, 305–314. https://doi.org/10.1002/jbio.201000069.
15. Messaraa, C.; Metois, A.; Walsh, M.; Hurley, S.; Doyle, L.; Mansfield, A.; O'Connor, C.; Mavon, A. Wrinkle and Roughness Measurement by the Antera 3D and Its Application for Evaluation of Cosmetic Products. *Skin. Res. Technol.* **2018**, *24*, 359–366. https://doi.org/10.1111/srt.12436.
16. Distante, F.; Bacci, P.A.; Carrera, M. Efficacy of a Multifunctional Plant Complex in the Treatment of the So-Called "Cellulite": Clinical and Instrumental Evaluation. *Int. J. Cosmet. Sci.* **2006**, *28*, 191–206. https://doi.org/10.1111/j.1467-2494.2006.00319.x.
17. Tomczak, M.; Tomczak, E. The Need to Report Effect Size Estimates Revisited. An Overview of Some Recommended Measures of Effect Size. *Trends Sport Sci.* **2014**, *21*, 19–25.
18. Emanuele, E.; Minoretti, P.; Altabas, K.; Gaeta, E.; Altabas, V. Adiponectin Expression in Subcutaneous Adipose Tissue Is Reduced in Women with Cellulite. *Int. J. Dermatol.* **2011**, *50*, 412–416. https://doi.org/10.1111/j.1365-4632.2010.04713.x.
19. Meglinski, I.V.; Matcher, S.J. Computer Simulation of the Skin Reflectance Spectra. *Comput. Methods Programs Biomed.* **2003**, *70*, 179–186. https://doi.org/10.1016/S0169-2607(02)00099-8.
20. Stamatas, G.N.; Zmudzka, B.Z.; Kollias, N.; Beer, J.Z. Non-Invasive Measurements of Skin Pigmentation in Situ. *Pigment. Cell Res.* **2004**, *17*, 618–626. https://doi.org/10.1111/j.1600-0749.2004.00204.x.
21. Lee, J.; Yoon, J. Assessment of Angle-Dependent Spectral Distortion to Develop Accurate Hyperspectral Endoscopy. *Sci. Rep.* **2022**, *12*, 11892. https://doi.org/10.1038/s41598-022-16232-0.
22. Cracowski, J.-L.; Roustit, M. Current Methods to Assess Human Cutaneous Blood Flow: An Updated Focus on Laser-Based-Techniques. *Microcirculation* **2016**, *23*, 337–344. https://doi.org/10.1111/micc.12257.

Disclaimer/Publisher's Note: The statements, opinions and data contained in all publications are solely those of the individual author(s) and contributor(s) and not of MDPI and/or the editor(s). MDPI and/or the editor(s) disclaim responsibility for any injury to people or property resulting from any ideas, methods, instructions or products referred to in the content.